# MICROSTRUCTURE ANALYSIS

Girard Simons

Physical Sciences, Incorporated

Prepared for:

Office of Naval Research
Advanced Research Projects Agency

15 August 1975

# QUARTERLY TECHNICAL REPORT

PERIOD: 1 MARCH 1975 to 1 JUNE 1975

## MICROSTRUCTURE ANALYSIS

Prepared for

OFFICE OF NAVAL RESEARCH
800 North Quincy Street
Arlington, Virginia 22217

27 June 1975

Prepared by

PHYSICAL SCIENCES INC.
18 Lakeside Office Park
Wakefield, Massachusetts 01880



Sponsored by

Advanced Research Projects Agency

ARPA Order No. 2961

QUARTERLY TECHNICAL REPORT

PERIOD: 1 MARCH 1975 to 1 JUNE 1975

| | |
|---|---|
| ARPA Order No. | 2961 |
| Program Code No. | 5E10 |
| Name of Contractor: | Physical Sciences Inc.<br>18 Lakeside Office Park, Wakefield, MA 01801 |
| Effective Date of Contract: | February 15, 1975 |
| Contract Expiration Date: | August 15, 1975 |
| Amount of Contract: | $51,081.00 |
| Contract No. | N00014-75-C-0927 |
| Principal Investigator | Girard Simons |
| Phone Number | (617) 245-7400 |
| Scientific Officer: | Office of Naval Research<br>Code 212<br>800 North Quincy Street<br>Arlington, Virginia 22217<br>Attn: CDR Donald D. Pizinger |
| Title: | MICROSTRUCTURE ANALYSIS |

Sponsored by

Advanced Research Projects Agency

ARPA Order No. 2961

# TASK I - OCEAN MICROSTRUCTURE

## I. INTRODUCTION

Field observations[1-3] have revealed that the ocean's thermocline possesses an internal structure consisting of a series of thin, laminar "sheets" of high gradient separated by "steps" of only moderate density gradient. The observed "microstructure" is represented schematically in Fig. 1. The step height H and the lateral extent of the observed structure varies widely over the range of mean density gradient indicated in Table I. The observation time refers to the time spent taking soundings at various lateral locations whereas the point persistence time refers to the time duration between soundings at a given lateral location.

Various mechanisms have been proposed to explain the observed phenomenon. These mechanisms consist of double diffusion,[4] interleaving,[5] internal gravity wave breaking[6] and internal wave steepening.[7] In this report, the concept of interval wave steepening is examined. We will first determine the set of admissable wave solutions and then examine the nonlinear coupling. Comparison with field data establishes the feasibility of the wave steepening approach.

Table I - Microstructure Data Base

| Observer | Grad $(\frac{\Delta\rho}{\rho})$ | H | Lateral Extent | Observation Time | Point Persistence Time |
|---|---|---|---|---|---|
| Howe & Tait | O ($10^{-6}$/m) | O (35 m) | O (10 mi) | 3 days | > 33 hrs |
| Simpson | O ($10^{-5}$/m) | O (10-20 m) | 1-3 km | 3 days | ? |
| Woods & Wiley | O ($10^{-4}$/m) | O (1-2 m) | ? | ? | ? |

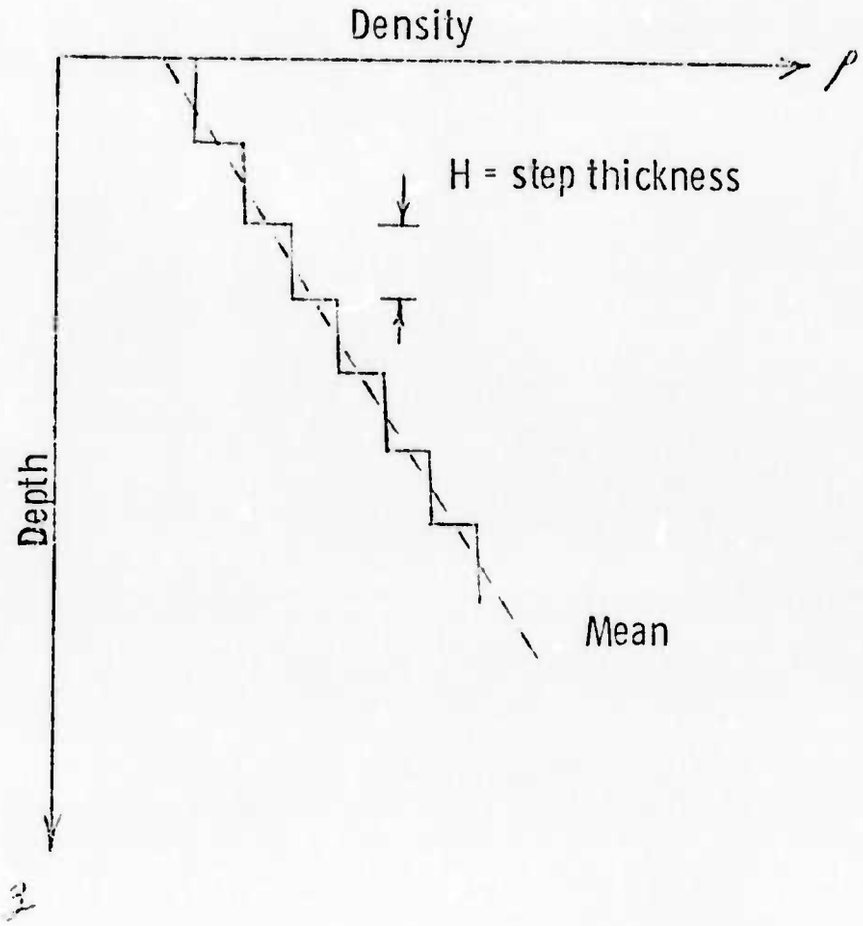


Figure 1 Ocean Microstructure

## II. INTERNAL GRAVITY WAVE MODEL

The equations of motion for a two-dimensional incompressible fluid are:

Incompressible:
$$\frac{D\tilde{\rho}}{D\tilde{t}} = 0 \tag{1}$$

Continuity:
$$\frac{\partial \tilde{u}}{\partial \tilde{x}} + \frac{\partial \tilde{v}}{\partial \tilde{y}} = 0 \tag{2}$$

where $\tilde{x}$ is the horizontal coordinate, $\tilde{y}$ is the vertical coordinate (positive upwards), and $\tilde{u}$ and $\tilde{v}$ represent the horizontal and vertical velocities respectively. The superscript ~ denotes a dimensional variable.

$\tilde{x}$ momentum:
$$\frac{\partial \tilde{u}}{\partial \tilde{t}} + \tilde{u}\,\frac{\partial \tilde{u}}{\partial x} + \tilde{v}\,\frac{\partial \tilde{u}}{\partial \tilde{y}} + \frac{1}{\tilde{\rho}}\,\frac{\partial \tilde{p}}{\partial x} + 0 \tag{3}$$

$\tilde{y}$ momentum:
$$\frac{\partial \tilde{v}}{\partial t} + u\,\frac{\partial \tilde{v}}{\partial \tilde{x}} + \tilde{v}\,\frac{\partial \tilde{v}}{\partial y} + \frac{1}{\tilde{\rho}}\,\frac{\partial \tilde{p}}{\partial \tilde{y}} + \tilde{g} = 0 \tag{4}$$

Equations (1) through (4) represent a model in which the density may be a function of temperature and salinity only

$$\tilde{\rho} = \tilde{\rho}\ (\tilde{s},\ \tilde{T}) \tag{5}$$

where the Lagrangian derivative of $\tilde{\rho}$, $\tilde{s}$ and $\tilde{T}$ are all zero.

The density profile in a static sea will be specified apriori

$$\frac{\partial \tilde{\rho}}{\partial \tilde{y}} = - \tilde{\beta}\ \tilde{\rho}_r \tag{6}$$

where $\tilde{\rho}_r$ is the reference density at $y = 0$. The value of $\tilde{\beta}$ is expressed in units of inverse length and has values between $10^{-4}$/m in the summer thermocline and $10^{-6}$/m in the deep sea. The influence of compressibility must be included for values of $\tilde{\beta}$ of the order of $5 \times 10^{-6}$/m. Thus, the incompressible model will be limited to the thermocline.

We expand the dependent variables into a static and wave contribution.

$$\tilde{\rho} = \tilde{\rho}_r + \tilde{\rho}_s (y) + \tilde{\rho}_w (\tilde{x},\ \tilde{y},\ \tilde{t}) \tag{7}$$

$$\tilde{p} = \tilde{p}_r - \tilde{\rho}_r\ \tilde{g}\ \tilde{y} + \tilde{p}_s (\tilde{y}) + \tilde{p}_w (\tilde{x}, \tilde{y}, \tilde{t}) \tag{8}$$

$$\tilde{v} = \tilde{v}_w\ (\tilde{x},\ \tilde{y},\ \tilde{t}) \tag{9}$$

$$\tilde{u} = \tilde{u}_w\ (\tilde{x},\ \tilde{y},\ \tilde{t}) \tag{10}$$

where we have restricted the analysis to zero mean shear. The only velocities are due to the wave contribution.

Setting all wave contributions equal to zero, we obtain the hydrostatic relationship between $\tilde{p}_s$ and $\tilde{\rho}_s$.

$$\frac{\partial \tilde{p}_s}{\partial \tilde{y}} = - \tilde{\rho}_s (\tilde{y})\ \tilde{g} \tag{11}$$

From (6) and (7), we specify $\tilde{\rho}_s$

$$\tilde{\rho}_s = - \tilde{\rho}_r \tilde{\beta} \tilde{y} \tag{12}$$

Substituting Equations (7) - (10) into (1) - (4) we will determine the equations of motion for the wave contribution. The equations are non-dimensionalized such that the linear terms are O (1). The reference variables are:

$$\tilde{\tau}_{ref} = \frac{1}{\tilde{\sigma}_o} \text{ where } \tilde{\sigma}_o = \sqrt{\tilde{g} \tilde{\beta}} \; \tilde{k}_H / \tilde{k}_v$$

$$\tilde{x}_{ref} = \frac{1}{\tilde{k}_H} = \frac{\tilde{\lambda}_H}{2\pi}$$

$$\tilde{y}_{ref} = \frac{1}{\tilde{k}_v} = \frac{\tilde{\lambda}_v}{2\pi}$$

$$\tilde{v}_{ref} = \tilde{v}_p \text{ (perturbation velocity)}$$

$$\tilde{u}_{ref} = \tilde{k}_v \tilde{v}_p / \tilde{k}_H$$

$$\tilde{\rho}_{ref} = \tilde{\beta} \tilde{v}_p \tilde{\rho}_r / \tilde{\sigma}_o$$

and

$$\tilde{p}_{ref} = \tilde{v}_p \tilde{\sigma}_o \tilde{k}_v \tilde{\rho}_r / \tilde{k}_H^2 .$$

The nondimensional equations of motion for the wave contribution are expressed as

$$\frac{\partial \rho_w}{\partial t} - v_w + \frac{\epsilon}{\delta} \left( u_w \frac{\partial \rho_w}{\partial x} + v_w \frac{\partial \rho_w}{\partial y} \right) \tag{13}$$

$$\frac{\partial u_w}{\partial x} + \frac{\partial v_w}{\partial y} = 0 \tag{14}$$

$$\frac{\partial p_w}{\partial x} + (1 - \alpha y + \frac{\alpha \varepsilon}{\delta} \rho_w) \left[ \frac{\partial u_w}{\partial t} + \frac{\varepsilon}{\delta} (u_w \frac{\partial u_w}{\partial x} + v_w \frac{\partial u_w}{\partial y}) \right] = 0 \tag{15}$$

$$\frac{\partial p_w}{\partial y} + \rho_w + \delta^2 (1 - \alpha y + \frac{\alpha \varepsilon}{\delta} \rho_w) \left[ \frac{\partial v_w}{\partial t} + \frac{\varepsilon}{\delta} (u_w \frac{\partial v_w}{\partial x} + v_w \frac{\partial v_w}{\partial y}) \right] = 0 \tag{16}$$

where the three dimensionless parameters are

$$\delta = \tilde{\lambda}_V / \tilde{\lambda}_H \tag{17}$$

$$\alpha = \tilde{\beta} / \tilde{k}_V \tag{18}$$

and

$$\varepsilon = \tilde{v}_p \tilde{k}_v / \sqrt{\tilde{g} \tilde{\beta}} \tag{19}$$

Microstructure data infers that both $\delta$ and $\alpha$ are much less than unity whereas $\varepsilon$ may be made small by choice of the perturbation velocity $\tilde{v}_p$. In the limit of all three parameters being small, the lowest order solution is given by the arbitrary sum of four plane waves.

Lowest Order Solution:

$$v_{w_o} = \sum_{s=\pm 1} \sum_{q=\pm 1} A_{s,q} \, e^{i(t + sx + gy)} \tag{20}$$

$$u_{w_o} = \sum_{s=\pm 1} \sum_{q=\pm 1} \left(\frac{-q}{s}\right) A_{s,q} \, e^{i(t + sx + gy)} \tag{21}$$

$$\rho_{w_o} = -i \sum_{s=\pm 1} \sum_{q=\pm 1} A_{s,q} \; e^{i(t + s x + g y)} \qquad (22)$$

$$p_{w_o} = \sum_{s=\pm 1} \sum_{q=\pm 1} q \, A_{s,q} \; e^{i(t + sx + qy)} \qquad (23)$$

where $A_{s,q}$ are arbitrary constants.

We seek a wave solution which propagates in the x direction and possesses structure in the y direction. Such a solution is obtained from equation (22).

$$\rho_{w_o} = \frac{1}{2} \; e^{i(t-x-y)} - \frac{1}{2} \; e^{i(t-x+y)} = -\sin y \; e^{i(t-x)} \qquad (24)$$

Equation (24) is a superposition of two plane transverse waves. The velocity perturbation from one family of waves will steepen the other family. This is unlike acoustic sound waves which are longitudinal waves and are self steepening.

In order to describe the steepening of the waves in equation (24), we must include the lowest order non-linear terms. Since the data shows

$$\delta = 0 \; (10^{-2})$$

and

$$\alpha = 0 \; (10^{-4})$$

we retain the $O(\epsilon/\delta)$ terms in equations (13) - (16).

$$\frac{\partial \rho_w}{\partial t} - v_w + \left(\frac{\epsilon}{\delta}\right)\left(u_w \frac{\partial \rho_w}{\partial x} + v_w \frac{\partial \rho_w}{\partial y}\right) = 0 \qquad (25)$$

$$\frac{\partial u_w}{\partial x} + \frac{\partial v_w}{\partial y} = 0 \tag{26}$$

$$\frac{\partial p_w}{\partial x} + \frac{\partial u_w}{\partial t} + \left(\frac{\epsilon}{\delta}\right)\left(u_w \frac{\partial u_w}{\partial x} + v_w \frac{\partial u_w}{\partial y}\right) = 0 \tag{27}$$

$$\frac{\partial p_w}{\partial y} + \rho = 0 \tag{28}$$

To solve equations (25)-(28), we seek a solution of the same form as the linear solution

$$\rho_w = \frac{1}{2}\left(e^{i\xi} - e^{i\eta}\right) \tag{29}$$

$$v_w = \frac{i}{2}\left(e^{i\xi} - e^{i\eta}\right) \tag{30}$$

$$u_w = -\frac{i}{2}\left(e^{i\xi} + e^{i\eta}\right) \tag{31}$$

$$p_w = -\frac{i}{2}\left(e^{i\xi} + e^{i\eta}\right) \tag{32}$$

where $\xi$ and $\eta$ are constant on their respective characteristics but the characteristic must be relocated as prescribed by the fluid velocity.

$$\xi = t - x - y + F(\xi, \eta) \tag{33}$$

$$\eta = t - x + y + G(\xi, \eta) \tag{34}$$

We first seek to describe $F(\xi,\eta)$ and $G(\xi, \eta)$ as a power series expansion in $(\epsilon/\delta)$

$$F(\xi, \eta) = \left(\frac{\epsilon}{\delta}\right) \xi_1(\xi, \eta) + \left(\frac{\epsilon}{\delta}\right)^2 \xi_2(\xi, \eta) \ldots \tag{35}$$

$$G(\xi, \eta) = \left(\frac{\epsilon}{\delta}\right) \eta_1(\xi, \eta) + \left(\frac{\epsilon}{\delta}\right)^2 \eta_2(\xi, \eta) \ldots \tag{36}$$

Substitution of (29) - (36) into the equations of motion (25) - (28), we obtain

$$\xi_1 = -\frac{1}{2} e^{i\eta} \tag{37}$$

$$\eta_1 = -\frac{1}{2} e^{i\xi} \tag{38}$$

$$\xi_2 = \frac{i}{4} e^{i\xi} e^{i\eta} \tag{39}$$

and

$$\eta_2 = \frac{i}{4} e^{i\xi} e^{i\eta} \,. \tag{40}$$

Equations (37) and (38) illustrate the nature of transverse wave steepening. The velocity perturbation from the $\eta$ waves is in the direction of propagation of the $\xi$ waves. Hence, the $\eta$ waves steepen the $\xi$ waves and vice versa.

The density profile associated with transverse wave steepening is obtained from equation (29). For convenience, we set $t - x = \pi/2$.

$$\rho_w = \sin y - \frac{1}{2}\left(\frac{\epsilon}{\delta}\right) \sin 2y + O\left(\frac{\epsilon}{\delta}\right)^2 \tag{41}$$

Equation (41) illustrates that steepening can occur only if $\delta \leq 0(\epsilon)$. Since $\epsilon$ is a small parameter, it is seen that steepening can occur only for small $\delta$

and this is in agreement with observations. The physical reason for the constraint on $\delta$ lies in the steepening mechanism for transverse waves. Since the $\eta$ waves steepen the $\xi$ waves and the $\tau_\eta$ waves are oscillatory, the $\xi$ waves must steepen within the oscillation time. Thus the perturbation velocity must disperse a wave its own wavelength in time $\tilde{t}_{ref}$. This is expressed as

$$\tilde{v}_p \; \tilde{t}_{ref} \geq \tilde{k}_v^{-1}$$

or

$$\delta \leq \epsilon \tag{42}$$

To solve for the characteristic locations for arbitrary values of $\epsilon/\delta$, we will expand F and G in higher harmonics of $e^{i\xi}$ and $e^{i\eta}$

$$F(\xi, \eta) = \sum_{m,n} A_{m,n} e^{im\xi + in\eta} \tag{43}$$

$$G(\xi, \eta) = \sum_{p,q} B_{p,q} e^{ip\xi + iq\eta} \tag{44}$$

Where $A_{m,n}$ and $B_{p,q}$ are constants to be related by the dynamic equations. This work will be carried out during the next quarter but the collective result of this quarter's effort may be compared to data to demonstrate that internal gravity wave steepening is a promising answer to the source of ocean microstructure.

## III. COMPARISON WITH DATA

While we have yet to demonstrate that steepening actually occurs, we have several constraints which must be consistent with observations of microstructure, otherwise steepening will never explain microstructure data.

The condition for steepening requires $\varepsilon = 0(\delta)$. This corresponds to

$$\tilde{v}_p = \frac{\tilde{k}_H}{\tilde{k}_V^2}\sqrt{\tilde{g}\,\tilde{\beta}} = \frac{\tilde{\lambda}_V^2\sqrt{\tilde{g}\,\tilde{\beta}}}{2\pi\,\tilde{\lambda}_H}$$

or, for the data in Table I,

$$\tilde{v}_p = 0\,(10^{-5}\ \text{m/sec}) \text{ to } 0\,(10^{-4}\ \text{m/sec})$$

and

$$\tilde{u}_{ref} = 0\,(1\text{-}2\ \text{cm/sec})\ .$$

Perturbation velocities of the order of cm/sec are not unlikely in the ocean. While observations demonstrate that $\delta$ is $0\,(10^{-2})$, the present theory demands only that $\delta$ be small compared to unity ($\delta \leq 0.1$).

Further constraints are placed on the solution by viscosity. We must insure that the inertia of the wave exceeds viscous damping. This is expressed as

$$\frac{\partial \tilde{u}_w}{\partial t} \geq \tilde{\nu}\,\frac{\partial^2 \tilde{u}_w}{\partial \tilde{y}^2}$$

or

$$\tilde{\lambda}_V^3 \geq \frac{(2\pi)^2\,\tilde{\nu}\,\tilde{\lambda}_H}{\sqrt{\tilde{g}\,\tilde{\beta}}} \qquad (15)$$

If the microstructure is formed by wave steepening $\tilde{\lambda}_v$ will correspond to the step height $\tilde{H}$ and must be smaller than the maximum stable step indicated in Fig. 2. The quantity $\tilde{\lambda}_H$ will correspond to the lateral extent of the microstructure and the wave period

$$\tilde{\tau}_p = \frac{2\pi}{\tilde{\sigma}_o} = \frac{2\pi}{\sqrt{\tilde{g}\,\tilde{\beta}}} \left(\frac{\tilde{\lambda}_H}{\tilde{\lambda}_V}\right) \tag{46}$$

is the persistence time of the microstructure. This is due to the fact that each family of waves is steepened by velocity perturbations from the opposite family which, in turn, is oscillatory. Hence, the microstructure will have the period $\tilde{\tau}_p$.

The analytic results are compared to the data of references 1 through 3 in Figs. 3 to 5 respectively. Figure 3 represents a set of conditions under which steepening is possible when $\tilde{\beta} = 0$ $(10^{-6}/m)$ and the data of Howe and Tait[1] lies within that window. The theory indicates that the structure should be stationary over a time period of weeks. The data shows that the microstructure was present and invarient for the observation period of days. Hence, there is no contradiction with data. Similar results are illustrated in Figs. 4 and 5. In all three cases the data falls within the "window" under which wave steepening is a possible explanation of microstructure.

Figure 2

STABILITY OF MICROSTRUCTURE

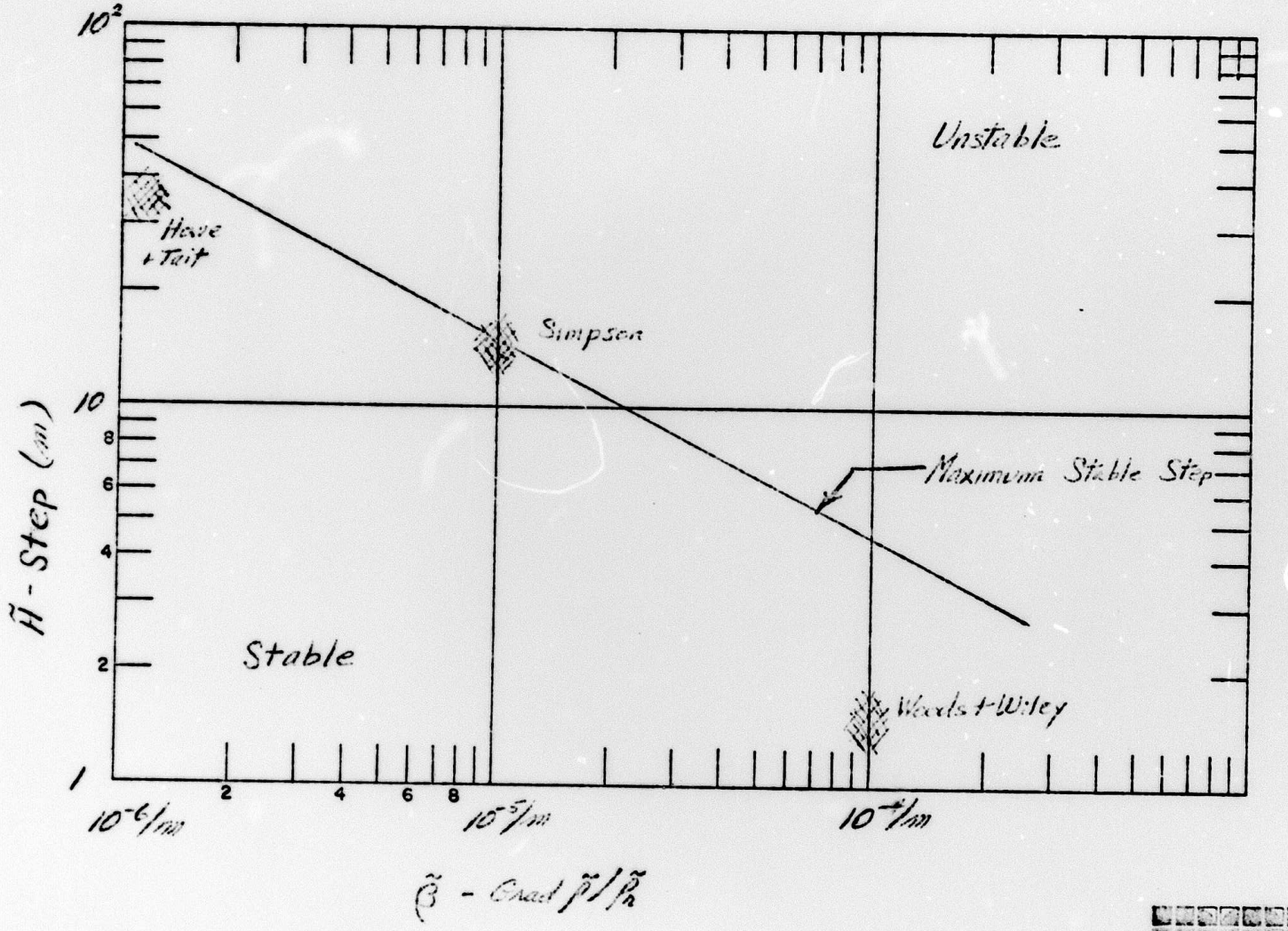

Figure 3

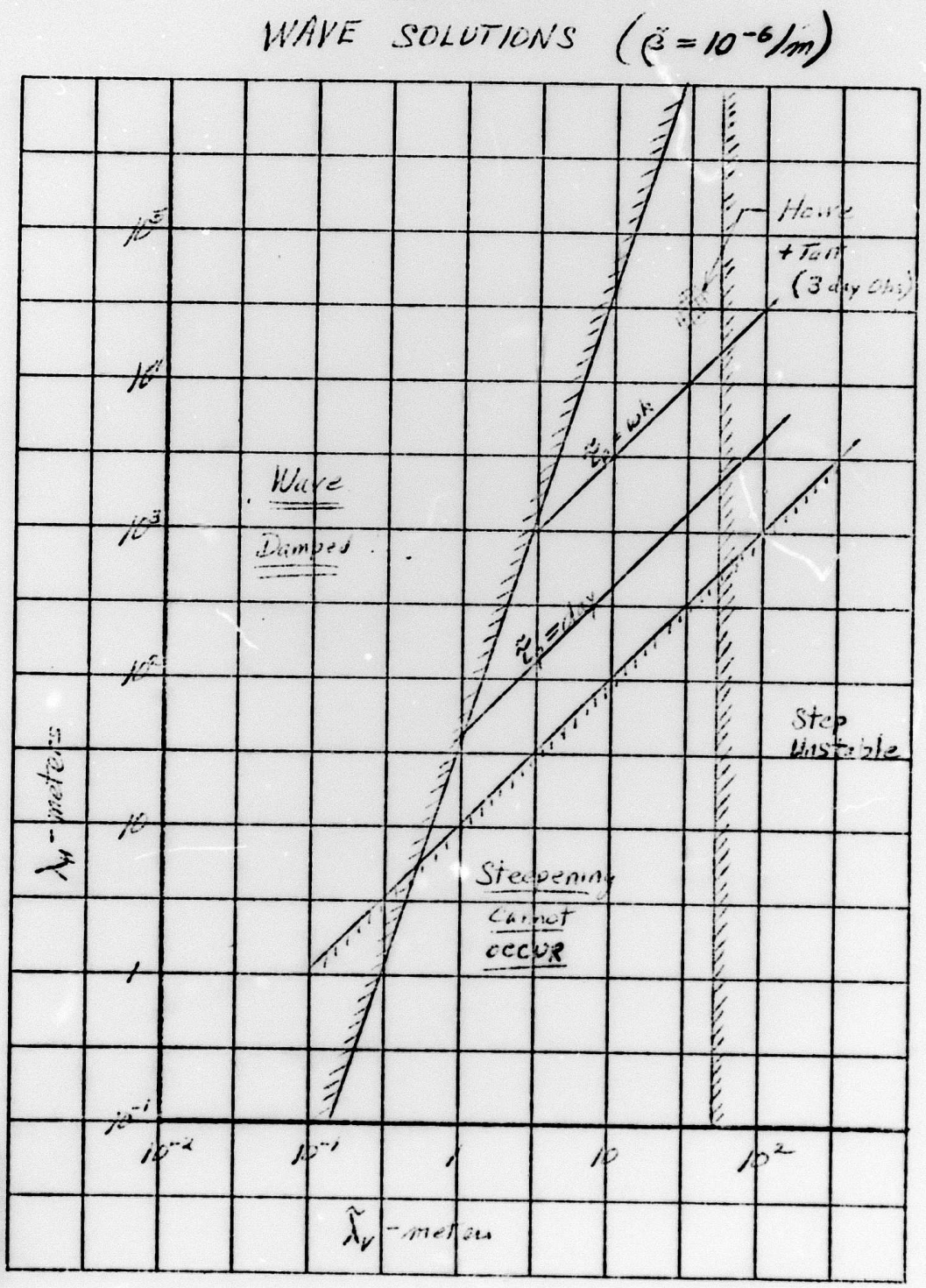
WAVE SOLUTIONS ($\tilde{\beta} = 10^{-6}$/m)
Wave Damped
Steepening Cannot occur
Step Unstable
Heave + Tilt (3 day obs)
$\lambda_w$ - meters
$\tilde{\lambda}_v$ - meters

Figure 4

WAVE SOLUTIONS ($\tilde{\beta} = 10^{-5}/m$)

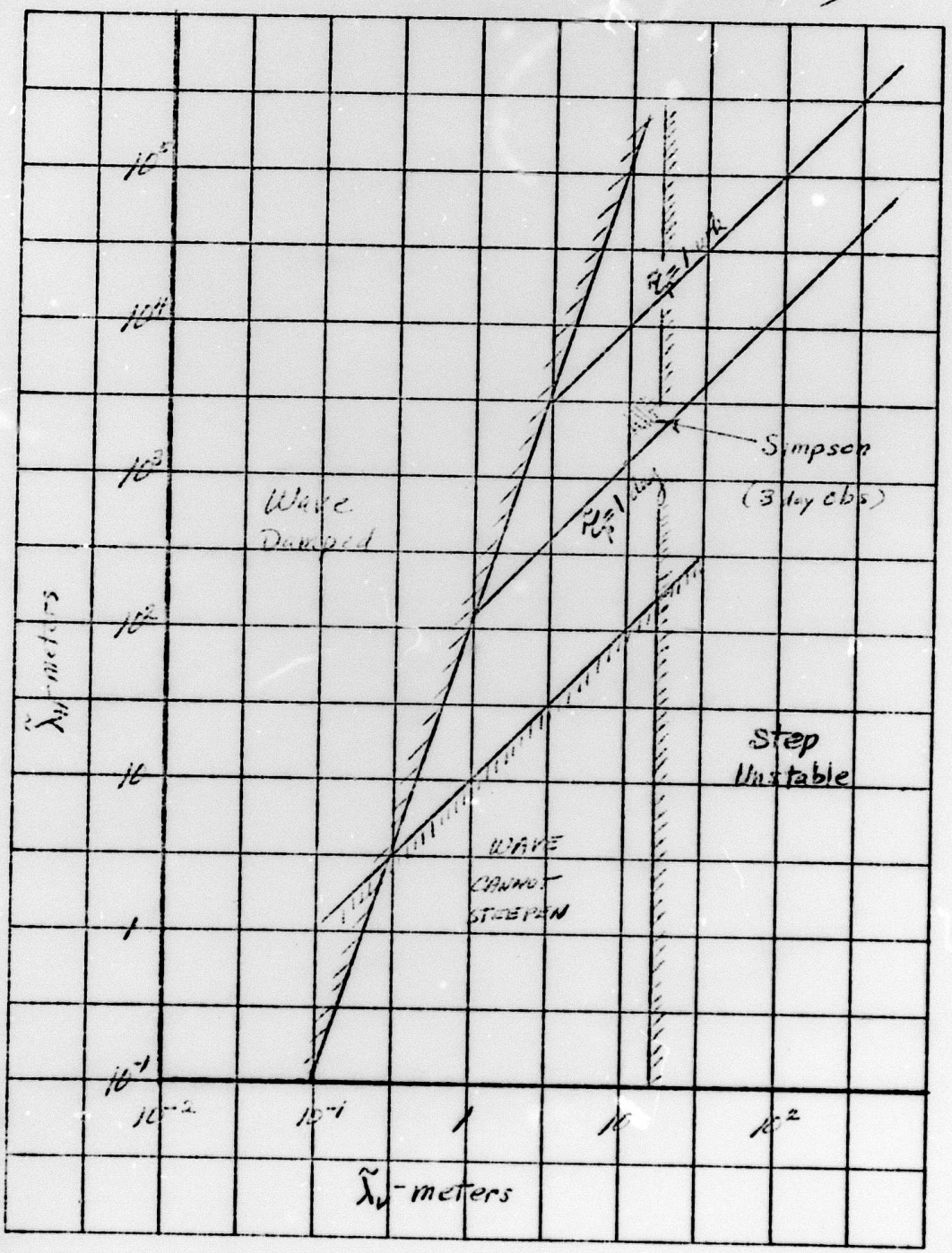

Figure 5

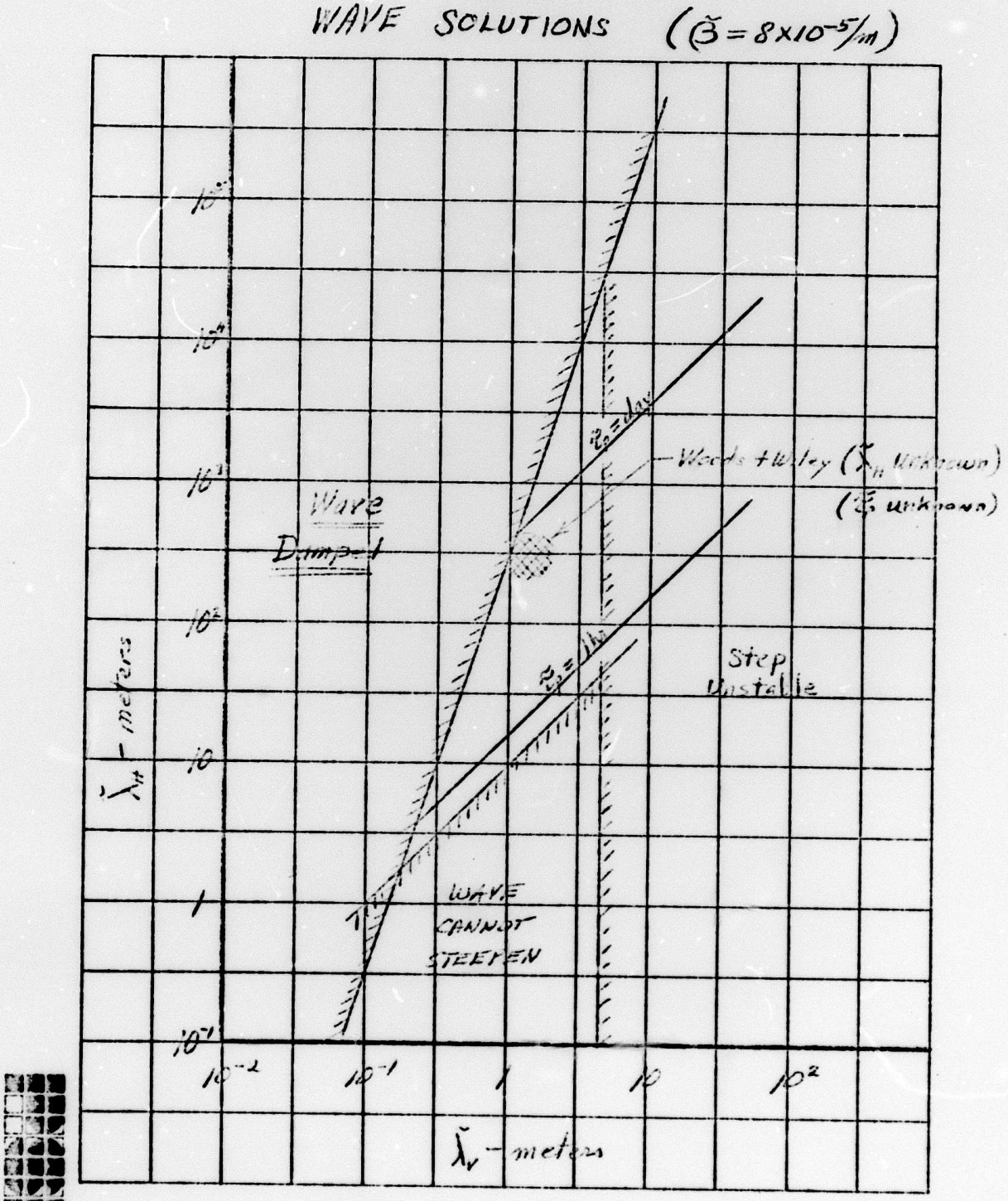
WAVE SOLUTIONS ($\tilde{\beta} = 8 \times 10^{-5}/m$)
Wave Damped
Woods + Wiley ($\tilde{\lambda}_h$ Unknown) ($\tilde{\lambda}_v$ Unknown)
Step Unstable
WAVE CANNOT STEEPEN
$\tilde{\lambda}_h$ - meters
$\tilde{\lambda}_v$ - meters
$10^{-2}$
$10^{-1}$
1
10
$10^2$

## IV. CONCLUSIONS AND FUTURE PLANS

The linearized gravity wave solution has demonstrated length and time scales consistent with field data. The conditions under which an undamped wave can steepen into a stable microstructure is also consistent with observations. Thus, internal gravity wave steepening appears to be a promising prospect for the source of ocean microstructure and the research during the next quarter will be devoted to demonstrating that steepening will result in the observed microstructure.

## TASK II - LASER SENSOR TECHNOLOGY ASSESSMENT

A variety of laser techniques for active, remote sensing of the atmosphere and ocean have been proposed. Some of these techniques involve Raman scattering, fluorescence, and electron spin resonance. From discussions with ARPA and IDA, the following areas have been selected for study: water temperature measurement and effluent detection using Raman Spectroscopy and magnetic anomaly detection using remote electron spin resonance (ESR) spectroscopy.

The general detection equations can be derived for each of the above techniques. Also, there are many sources of measurement degradation which must be considered in any specific scenario. It is the purpose of this study to try to establish and document the physical limitations of the detection processes.

The first area to be studied is Raman spectroscopy. It is well known that Raman spectroscopy is a very selective, yet insensitive, technique for remote detection of gaseous or liquid molecules and atoms. The general principle in the Raman scattering process is that the scattered light is wavelength shifted by an amount dependent on the atomic or molecular structure of the scatterer. Thus, identification of the scatterer is possible.

A numerical example will be discussed to illustrate a typical example. Let the remote system be 300 m from the scattering center, and the collecting mirror be 35 cm in diameter. Thus, the solid angle of the receiving system is $10^{-6}$ steradians. A typical Raman cross-section is $10^{-31}$ $cm^2$/ster. The optical efficiency of the detection system will be assumed to be $10^{-1}$ for ocean surface detection. The attenuation of the laser beam and scattered beam must be included for sub-surface detection. Using the detection equation,[8] the probability of receiving a Raman scattered photon per molecule for each photon transmitted is $10^{-38}$.

To obtain the total probability, the number $10^{-38}$ is multiplied by the number of scattering molecules in the resolution volume. Taking an example of a 1 $m^3$ resolution volume with $10^{16}$ scattering molecules/cc, the total probability is $10^{-16}$. Thus, per joule of green light, approximately 100 Raman scattered photons would be received. As a reference, an average power of 1 watt at 5030 Å is a reasonable bench mark number for today's commercial laser technology. However, visible lasers with about 100 watts of average power are under development at several laboratories.[9] Maps will be provided in the final report analyzing the broad range of possible systems parameters applicable for effluent detection.

Raman spectroscopy has been shown to be capable of measuring water temperature, because the structure of liquid water is temperature dependent.[10,11] Experimental work and analysis by Chang and Young have demonstrated the feasibility of this concept in the laboratory.[11] However, field systems appear to be impractical based on todays' visible laser technology. Ways to enhance the Raman scattered signal are desired to reduce the required average laser power.

Stimulated Raman scattering (SRS) and resonant Raman scattering are two proven techniques to obtain much higher scattering efficiencies under some conditions. It is part of our program plan to assess the applicability of these techniques.

Recent work by Dheer et al has examined the stimulated Raman spectra of $H_2O$.[12] Radiation levels of $\gg 100$ Mw/$cm^2$ appear to be necessary to exeeed the threshold for stimulated Raman scattering. The need for high flux levels puts greater demands on a system than a spontaneous Raman system because of larger peak power requirements. Besides the high flux level requirements, the SRS spectra is narrower than the spectra of spontaneous Raman scattering because of a gain phenomena associated with SRS.[13] The change in spectra may influence the sensitivity of the temperature measurement process and needs to be evaluated.

Our preliminary conclusion is that a remote field system utilizing stimulated Raman scattering to measure water temperature may not provide any advantage over the use of ordinary Raman scattering techniques. After further study a more

detailed conclusion based on physical limitations will be made in the final report.

During the next quarterly period work will be initiated on investigating the use of SRS and Resonance Raman Enhancement to determine the fundamental limitations of this technology to the detection of various species such as oil, $H_2$, and other species in sea water. In addition, the feasibility of ESR spectroscopy to remotely detect small changes in the earth's magnetic field will be studied. The conclusion of both of these analyses will be included in the Contract Final Report.

## REFERENCES


1. M. R. Howe and R. I. Tait, "Further Observations of Thermo-haline Stratification in the Deep Ocean," Deep Sea Research, 1970, Vol. 17, pp. 963 to 972.

2. J. H. Simpson, "Density Stratification and Microstructure in the Western Irish Sea", Deep Sea Research, 1971, Vol. 18, pp. 309 to 319.

3. J. D. Woods, "Wave-Induced Shear Instability in the Summer Thermocline", J. Fluid Mech. (1968), Vol. 32, Part 4, pp. 791-800.

4. M. E. Stern and J. S. Turner, "Salt Fingers and Convecting Layers", J. Fluid Mech. 16, 497-511, 1969.

5. H. Stommel and K. N. Fedorov, "Small Scale Structure in Temperature and Salinity Near Timor and Mindanao", Tellus, 19, (2) 307-325.

6. J. D. Woods and R. L. Wiley, "Billow Turbulence and Ocean Microstructure", Deep-Sea Research, 1972, Vol. 19, pp. 87-121.

7. I. Orlanski and K. Bryan, "Formation of the Thermodine Step Structure by Large-Amplitude Internal Gravity Waves", J. Geophysical Research, Vol. 74, No. 28, Dec. 20, 1969, pp. 6975-6983.

8. Laser Raman Gas Diagnostics, M. Lapp and C. Penny Editors (Plenum Press, New York, 1974).

9. 1975 IEEE/OSA Conference on Laser Engineering and Applications, Washington, D.C., May 28-30, 1975.

10. G. E. Walrafen, J. Chem. Phys. 47, 114, (1967).
G. E. Walrafen, J. Chem. Phys. 48, 244, (1968).

11. Chin H. Chang and Lee A. Young, "Sea Water Temperature Measurement from Raman Spectra", Contract No. N62269-73-C-0073, Research Note 960, Avco Everett Research Laboratory Inc., Everett, Mass. 02149.

12. M. K. Dheer, D. Madhaven, D. Ramachandra Rao, Chem. Phys. Lett. 32, 341, (1975).

13. A. Yariv, Quantum Electronics, (Wiley, New York, 1968).